

Engineered Ionizable Side Chains

Gisela D. Cymes and Claudio Grosman

Abstract One of the great challenges of mechanistic ion-channel biology is to obtain structural information from well-defined functional states. In the case of neurotransmitter-gated ion channels, the open-channel conformation is particularly elusive owing to its transient nature and brief mean lifetime. In this Chapter, we show how the analysis of single-channel currents recorded from mutants engineered to contain single ionizable side chains in the transmembrane region can provide specific information about the open-channel conformation without any interference from the closed or desensitized conformations. The method takes advantage of the fact that the alternate binding and unbinding of protons to and from an ionizable side chain causes the charge of the protein to fluctuate by 1 unit. We show that, in mutant muscle acetylcholine nicotinic receptors (AChRs), this fluctuating charge affects the rate of ion conduction in such a way that individual proton-transfer events can be identified in a most straightforward manner. From the extent to which the single-channel current amplitude is reduced every time a proton binds, we can learn about the proximity of the engineered side chain to the lumen of the pore. And from the kinetics of proton binding and unbinding, we can calculate the side-chain's affinity for protons (pK_a), and hence, we can learn about the electrostatic properties of the microenvironment around the introduced ionizable group. The application of this method to systematically mutated AChRs allowed us to identify unambiguously the stripes of the M1, M2 and M3 transmembrane α -helices that face the pore's lumen in the open-channel conformation in the context of a native membrane.

Keywords Nicotinic receptor • Acetylcholine receptor • Single-molecule electrophysiology • Ion-channel electrostatics • Acid-base chemistry • Proton transfer

C. Grosman (✉) · G. D. Cymes
Department of Molecular and Integrative Physiology, Center for Biophysics and
Computational Biology, Program in Neuroscience, University of Illinois at
Urbana-Champaign, Urbana, IL, USA
e-mail: grosman@illinois.edu

C. Grosman
524 Burrill Hall, 407 S. Goodwin Ave, Urbana, IL 61801, USA Claudio Grosman

© Springer Science+Business Media New York 2015
C. Ahern, S. Pless (eds.), *Novel Chemical Tools to Study Ion Channel Biology*,
Advances in Experimental Medicine and Biology 869,
DOI 10.1007/978-1-4939-2845-3_2

1 Introduction

Ion channels owe their central role in cell physiology to their ability to change conformation in a manner that depends on their environment. Certainly, the probability of ligand-gated ion channels being “open” (that is, the probability of the channel adopting the ion-conductive conformation) increases upon agonist binding, whereas the open probability of voltage-gated ion channels depends on the membrane potential and that of mechanosensitive channels depends on the extent to which the membrane is stretched. For several years now, a major goal of basic ion-channel research has consisted of characterizing the different physiologically relevant conformations of these membrane proteins in terms of three-dimensional structures.

A number of experimental approaches to ion-channel structure have been applied, each one with its own advantages and limitations. X-ray crystallography, for example, has the clear advantage that it can provide structural information with atomic resolution, but the method has been mainly applied to detergent-solubilized channels, and there seems to be no reason why an ion channel extracted from a membrane should behave in the same way as it does when embedded in it. On the other hand, although cryo-electron microscopy can be applied to membranes containing ion channels, the approach usually provides coarser structural information (although remarkable advances in this regard have recently been made; Liao et al. 2013). Importantly, these direct structural methods do not allow for the simultaneous monitoring of function, and hence, the conformational state of the channel has to be inferred from the conditions used during the preparation of the imaged samples or, simply, from the way the structural models look like. Conversely, methods that do allow for the simultaneous study of functional and structural properties of ion channels in their native environment—such as the substituted-cysteine accessibility method (SCAM), and voltage-clamp fluorometry—require that the structural information be inferred from electrophysiological or fluorescence observations, and thus, the insight is indirect and of low resolution. Moreover, ensemble (as opposed to single-molecule) implementations of these indirect methods often suffer from the fact that the signal is contributed by different conformations of the channel because only under extreme conditions do channels populate a defined single conformation. For example, in the case of (wild-type) neurotransmitter-gated ion channels, the complete absence of neurotransmitter is required to ensure a high occupancy of the closed-channel conformation, whereas a saturating concentration of neurotransmitter is needed to bias the population of channels toward the desensitized conformation at equilibrium. However, at any concentration of neurotransmitter between zero and saturating, all three physiologically relevant conformations of the channel—closed, open and desensitized—coexist in a mixture, and no concentration of agonist exists that can keep most of the channels in the open-channel conformation for longer than a few tens of milliseconds.

It was precisely to overcome the elusiveness of the open state that we developed the single-molecule approach we describe in this Chapter. Being a single-channel method, the identification of the time intervals during which the channel adopts the open-channel conformation (rather than the closed or desensitized conformations) is both straightforward and unequivocal. As a probe of the local environment, the approach uses ionizable amino acids systematically substituted (one at a time) at transmembrane positions of individual subunits. The use of these genetically encoded reporter groups avoids the difficulties and uncertainties that typically accompany the use of covalently attached labels, whereas the use of naturally occurring ionizable side chains avoids the complications associated with the use of unnatural amino-acid mutagenesis. Also, because the observable consists of the effect of the protonatable side-chain's fluctuating charge on the amplitude of single-channel currents, the required equipment is reduced to a patch-clamp setup and the recorded signals are reduced to current traces. Indeed, the distinctive feature of the approach we are presenting here is that both structure and function are inferred from the same type of observation: a single-channel recording.

2 The Method: Rationale, Previous Results, and Practical Implementation

Proton-Transfer and Ion Channels Every time a proton binds to or unbinds from an amino-acid side chain, the charge of the protein fluctuates by 1 unit; the binding of a proton to a basic side chain adds one positive charge, whereas the binding of a proton to an acidic side chain eliminates a negative charge. Thus, when ionizable side chains are located close to a channel's ion-permeation pathway, these "tethered" charges are expected to interact electrostatically with the passing ions in such a way that the transit of ions through the channel is either accelerated or retarded. In other words, the binding and unbinding of individual protons to and from the channel are expected to manifest as discrete changes in the amplitude of the single-channel current. This is exactly what we observed in our work on mutants of the adult-type muscle nicotinic acetylcholine receptor (AChR; Fig. 1) engineered to contain single ionizable side chains in the transmembrane-pore domain (Cymes et al. 2005; Cymes and Grosman 2008, 2011). In this non-selective cation channel (a heteropentamer of two $\alpha 1$ and one each of $\beta 1$, δ and ϵ subunits), we found that protonation of basic side chains decreases, whereas deprotonation of acidic side chains increases, the size of the unitary currents. Thus, as protons bind and unbind to and from engineered basic side chains, the open-channel current alternates between a "*sublevel*" and a "*main level*" (Fig. 2), whereas, in the case of acidic side chains, the current alternates between a *main level* and a "*superlevel*" (Fig. 3).

We decided to take advantage of this phenomenon and use it systematically to obtain structural information (however indirect) about the AChR with the absolute certainty that the observed signal arises exclusively from the open-channel confor-

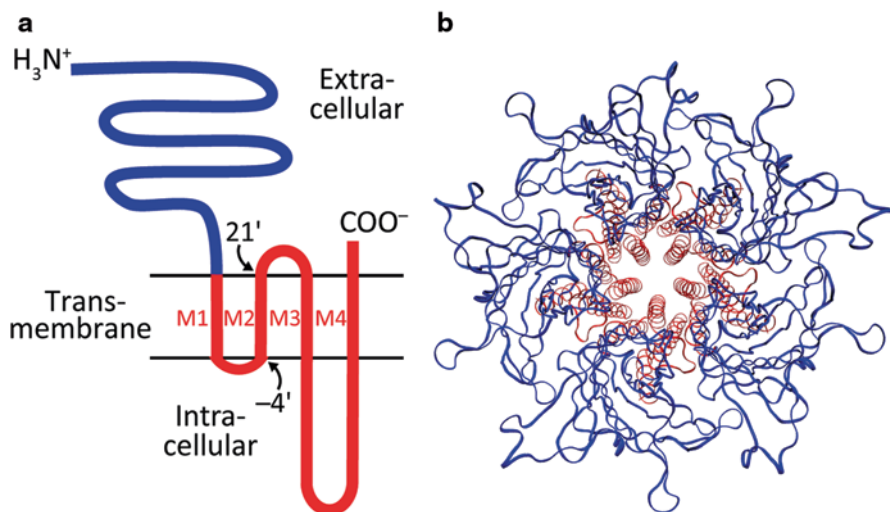


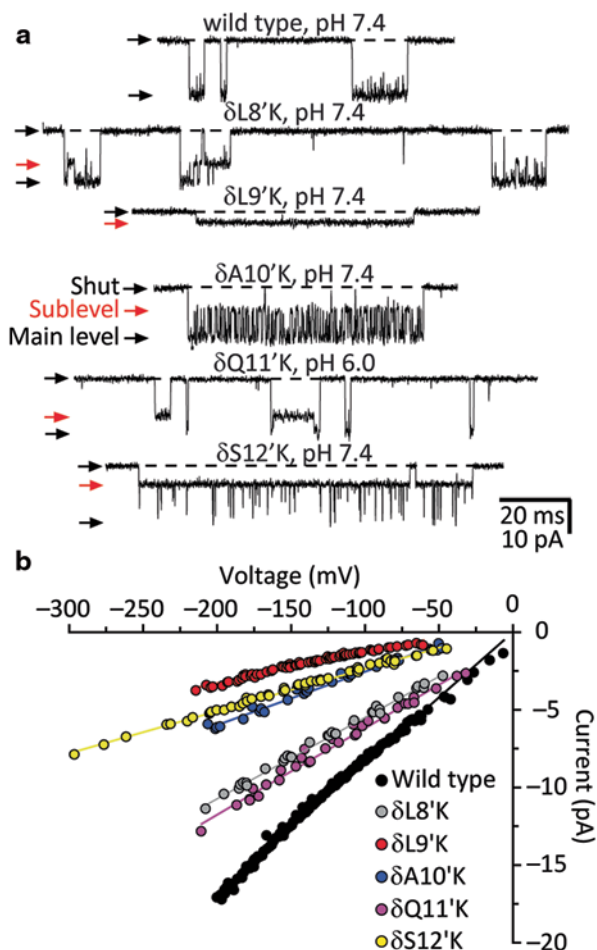
Fig. 1 The nicotinic acetylcholine receptor. **a** Membrane topology of each subunit of members of the pentameric ligand-gated ion-channel superfamily. Residues in and flanking the M2 α -helix are numbered using a prime-notation system that assigns position 0' to the conserved basic residue near its (intracellular) N-terminus; positions -4' and 21' mark the ends of this helix. **b** Ribbon representation of GLIC, a bacterial member from *Gloeobacter violaceus* (PDB ID code: 3EAM; Bocquet et al. 2009) as viewed from the extracellular side. The color code is the same as in (a). The M3–M4 linker of GLIC is much shorter than that of pentameric ligand-gated ion channels from animals

mation. Of course, because ion currents do not flow through the non-conductive conformations, proton binding and unbinding to and from the closed or desensitized states of the channel go undetected, and hence, do not contribute to our observations.

Single-Channel Experiments Single-channel current recordings contain two types of information—current amplitude and time—and, in the framework of this method, structural insight can be inferred from the analysis of both of them (Fig. 4).

Consistent with what is expected from an electrostatic interaction, we found that the extent to which the binding of a proton decreases the current amplitude of the muscle AChR depends on the proximity of the protonated side chain to the long axis of the pore. Indeed, we found that, on average, protonation of basic side chains engineered on the pore-lining M2 α -helices (Cymes et al. 2005) reduces the current amplitude more than does protonation of basic side chains engineered on the peripheral, non-pore-lining M1 and M3 α -helices (Cymes and Grosman 2008). We used this distance dependence to estimate the rotational angle of the AChR's M1, M2 and M3 α -helices with respect to the ion-permeation axis in the open-channel conformation. When we engineered single lysines along the entire M2 α -helix of the muscle AChR's δ subunit (see Fig. 2a for some example positions), we found that the extent to which the single-channel conductance is reduced upon protonation of the introduced lysines (Fig. 2b) displays the periodicity of a α -helix (Fig. 5).

Fig. 2 Protonation of engineered lysines slows down cation conduction. **a** Single-channel inward currents (cell-attached configuration; ~ -200 mV; 10-mM pH-buffer; 1- μ M ACh) recorded from HEK-293 cells transiently expressing the indicated muscle-AChR constructs. The indicated pH values are those of the pipette solution. Openings are downward deflections, and display $fc \approx 6$ kHz. “Shut” denotes the zero-current level. “Main level” denotes the open-channel current level having a wild type-like conductance. **b** Single-channel current–voltage (i – V) relationships for the five δ -subunit mutants in **a** and the wild-type AChR. For clarity, only the i – V curve corresponding to the sublevel is shown for the mutants. (Reproduced from Cymes et al. 2005)



This result allowed us to identify the stripe of the M2 α -helix that faces the lumen in the open-channel conformation (Cymes et al. 2005). Similarly, application of this method to the M1 and M3 α -helices led us to identify their pore-facing stripes when the channel is open (note that ionizable side chains need not face the lumen of the pore directly to exert a measurable electrostatic effect on the passing currents; Cymes and Grosman 2008). We have not yet extended our studies to the M4 α -helix, the most peripheral transmembrane segment.

Extent of Channel Block The values of extent of channel block in Fig. 5 were calculated as the difference between the inward conductances of the main level and the sublevel divided by the conductance of the main level, and hence, these values are in the 0–1 range. However, at several positions, the presence of a lysine seemed

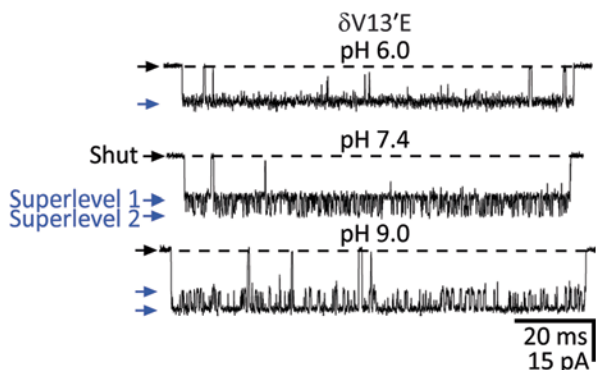


Fig. 3 Deprotonation of engineered glutamates speeds up cation conduction. Single-channel inward currents (cell-attached configuration; ~ 100 mV; 10-mM pH-buffer; 1- μ M ACh) recorded from HEK-293 cells transiently expressing the indicated mutant at position 13' of the AChR's δ subunit. The indicated pH values are those of the pipette solution. To increase the signal-to-noise ratio, the construct also carried two mutations in the ϵ subunit: a glutamine-to-glutamate mutation at position -1' and the deletion of the extra glycine at position -3'. These ϵ -subunit mutations increase the single-channel conductance by ~ 50 pS (*superlevel 1*). The deprotonation of the glutamate engineered at $\delta 13'$ increases the conductance even further, by another step of ~ 50 pS (*superlevel 2*). Openings are downward deflections, and display $f_c \approx 6$ kHz. "Shut" denotes the zero-current level. The pK_a of the glutamate side chain substituted at position 13', averaged across patches, was calculated to be 7.88 ± 0.01 , which represents an up-shift of ~ 3.5 units with respect to the bulk-water value of ~ 4.4 . The glutamates at position -1' remain deprotonated in the 6.0–9.0 pH range. (Reproduced from Cymes and Grosman 2012)

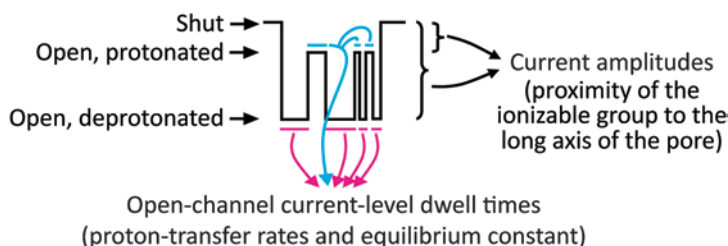


Fig. 4 Schematic single-channel trace with fluctuating open-channel current levels. This scheme summarizes the rationale behind our approach. In the muscle AChR, the binding of protons to basic or acidic side chains attenuates the amplitude of the single-channel currents

to "lock" the open-channel current at a sublevel even at pH 9.0 (see for example the case of position 9' in Fig. 6a)—as if the lysine were protonated all the time—and therefore, the single-channel conductance of the main level could not be estimated; in these cases, the main-level conductance was assumed to be that of the wild-type channel.

To be more rigorous, however, we also engineered histidines at these positions. Because of its lower affinity for protons in bulk solution ($pK_{a \text{ His}} \approx 6.4$; $pK_{a \text{ Lys}} \approx 10.4$), the side chain of a histidine is likely to bind protons less tightly than does the side chain of a lysine also when engineered in a protein, and thus, we expected

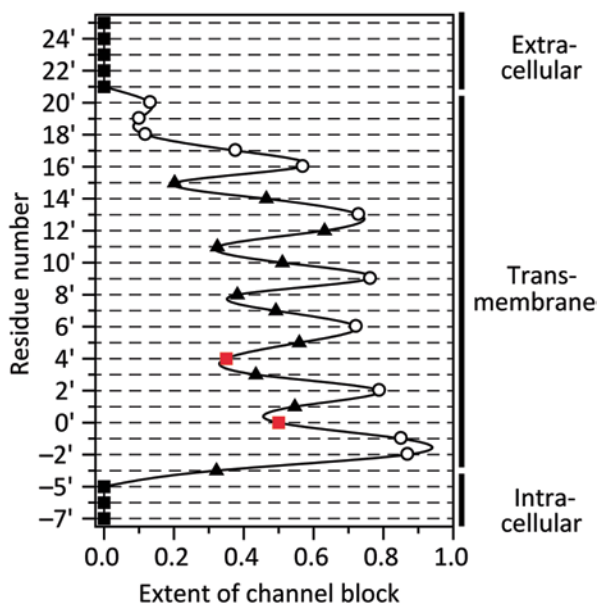


Fig. 5 Extent of channel block exerted by systematically engineered lysines. The plot corresponds to the δ subunit of the muscle AChR. The values of extent-of-channel block were calculated as the difference between the inward conductances of the *main level* and the *sublevel* divided by the conductance of the main level. Thus, “1” corresponds to complete block, whereas “0” corresponds to no block. The *unbroken line* is a cubic-spline interpolation. As judged from the extent of block, the data suggest that the lumen of the open-channel pore is to the *right* of the plot. Note that, even at positions that would be on the backside of the α -helix (such as 8', 11' and 15'), lysines exerted a considerable electrostatic effect on the cation current. *White circles* denote lysine mutants whose open-channel currents stayed at a sublevel even at pH 9.0; *black triangles* denote lysine mutants whose open-channel current interconverted between a *main level* and a *sublevel* in the 6.0–9.0 pH range; and *black squares* denote lysine mutants whose open-channel currents stayed at the main level even at pH 6.0. The latter was the case for positions outside the thickness of the membrane, but also, for positions 0' and 4'. Because these two positions are flanked by positions at which lysines did block the currents, we present them in *red* and assign them tentative extent-of-block values predicted on the basis of the values observed at neighboring positions. In the δ subunit, there is only one residue (not two) between positions -2' and -5'; this is also the case for subunits $\alpha 1$ and $\beta 1$. Only the ϵ (and γ) subunit has residues at both, positions -3' and -4'. (Reproduced from Cymes et al. 2005)

histidines to reveal the conductance of the main level at positions where substituted lysines failed. Indeed, this was the case for our experiments (see, for example, Fig. 6b–d), and importantly, extent-of-block values estimated for histidines were similar to those estimated for lysines. Figure 7 shows the case of position 12', where the pK_a of an engineered lysine is 8.87 ± 0.008 (and hence, $\Delta pK_a = pK_a - pK_{a, \text{bulk}} = 8.87 - 10.4 = -1.53$ units). On the other hand, a histidine engineered at this same position (Fig. 7b) seemed to remain deprotonated all the time, even at pH 6.0, which would not be surprising if the pK_a of this histidine were as downshifted

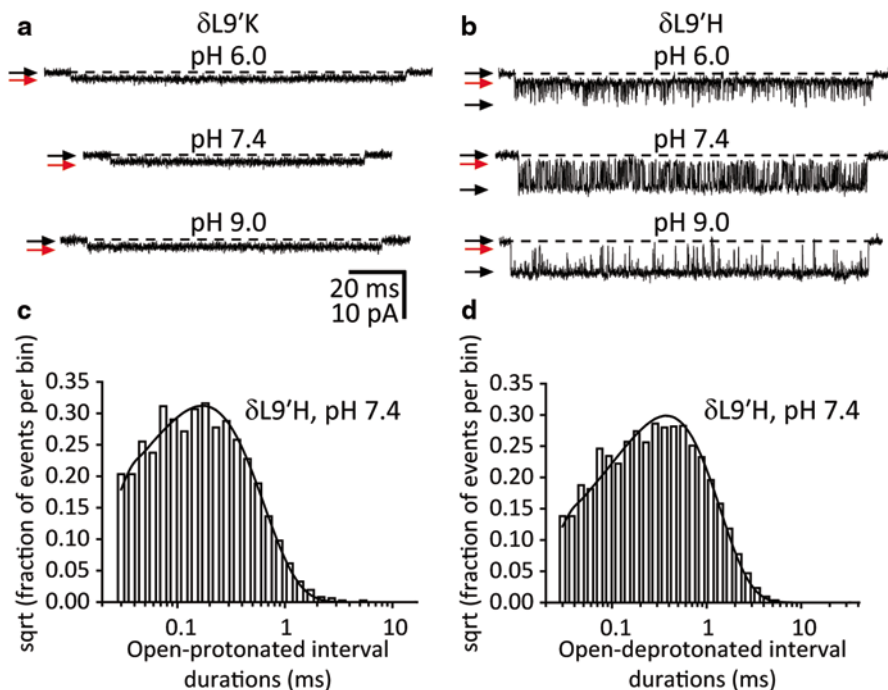


Fig. 6 Protonation–deprotonation events at position 9'. **a, b** Single-channel inward currents (cell-attached configuration; ~ -100 mV; 10-mM *pH*-buffer; 1- μ M ACh) recorded from HEK-293 cells transiently expressing the indicated mutants at position 9' of the AChR's δ subunit. The indicated *pH* values are those of the pipette solution. Openings are downward deflections, and display $fc \approx 6$ kHz. The color code for the arrows is the same as in Fig. 2, and the calibration bars are the same for both panels. **c, d** Dwell-time histograms of the protonated and deprotonated open-channel current levels corresponding to one representative recording at *pH* 7.4 from the histidine mutant (number of shut and open intervals=316,245). Shut-time histograms are not shown. *Unbroken lines* are monoexponential densities computed from the estimates of transition rates with allowance for missed events (time resolution=25 μ s). Transition rates were estimated from maximum-likelihood fitting of dwell-time series with kinetic models containing two interconverting open states of different conductance. The pK_a of the histidine substituted at this position, averaged across patches, was calculated to be 7.10 ± 0.004 , which represents a modest up-shift of ~ 0.7 units with respect to the bulk-water value of ~ 6.4 . This up-shift may explain why a lysine substituted at this position remains protonated even at *pH* 9.0. (Reproduced from Cymes et al. 2005)

as that of a lysine at this position. Positions 1' and 10', also on the sides of M2, displayed a similar acid–base behavior (Fig. 8).

As for arginine, we engineered this residue at much fewer transmembrane positions, and therefore, our data for this side chain are more limited. At most of these positions, however, the mutated arginine caused the open-channel current signal to dwell permanently in a sublevel (of nearly the same conductance as that of the sublevel observed for a lysine or a histidine engineered at the same position) without any detectable excursion to a current level of higher conductance. Again, interpreting sojourns in the sublevel as intervals during which the ionizable side chain is

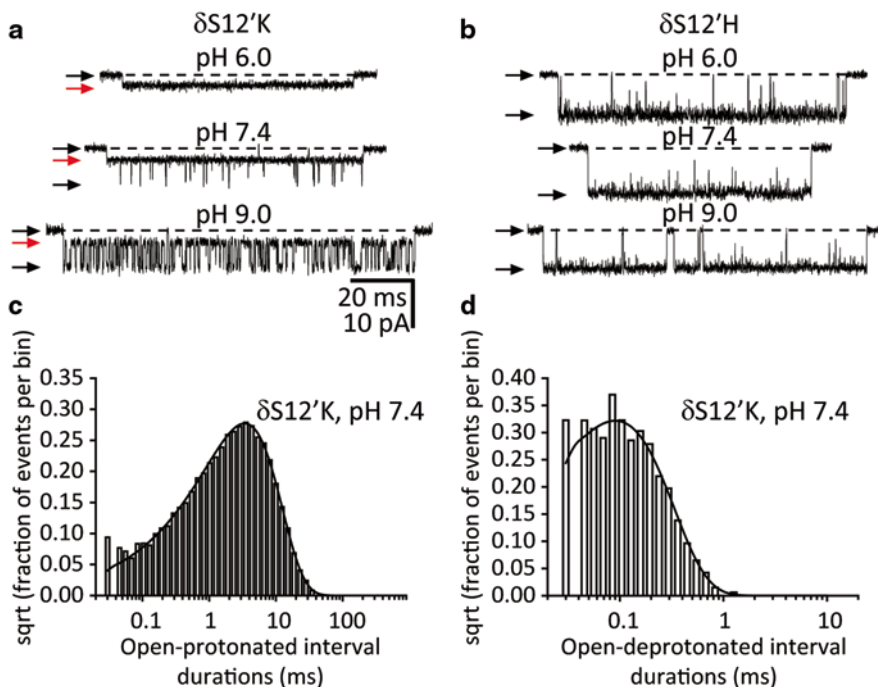


Fig. 7 Protonation–deprotonation events at position 12'. **a, b** Single-channel inward currents (cell-attached configuration; ~ 100 mV; 10-mM *pH*-buffer; 1- μ M ACh) recorded from HEK-293 cells transiently expressing the indicated mutants at position 12' of the AChR's δ subunit. The indicated *pH* values are those of the pipette solution. Openings are downward deflections, and display $f_c \approx 6$ kHz. The color code for the arrows is the same as in Fig. 2, and the calibration bars are the same for both panels. **c, d** Dwell-time histograms of the protonated and deprotonated open-channel current levels corresponding to one representative recording at *pH* 7.4 from the lysine mutant (number of shut and open intervals = 58,450). Shut-time histograms are not shown. Unbroken lines are monoexponential densities computed from the estimates of transition rates with allowance for missed events (time resolution = 25 μ s). Transition rates were estimated from maximum-likelihood fitting of dwell-time series with kinetic models containing two interconverting open states of different conductance. The pK_a of the lysine substituted at this position, averaged across patches, was calculated to be 8.87 ± 0.008 , which represents a down-shift of ~ 1.5 units with respect to the bulk-water value of ~ 10.4 . This down-shift may explain why a histidine substituted at this position remains deprotonated even at *pH* 6.0. (Reproduced from Cymes et al. 2005)

protonated, this finding is entirely consistent with the high pK_a value of the guanidine group of arginine in bulk solution ($pK_{a, \text{Arg}} \approx 12.5$) and the well-known high energetic cost of abstracting a proton from it even in the most hydrophobic protein environments. Owing to this extremely high affinity for protons, we found arginines to be of little use in the context of our approach.

A reduction of the single-channel conductance was not the only effect of the engineered protonated basic side chains. At several positions, a leftward shift of the rectilinear portion of the current–voltage (i – V) relationships (in the inward direction) could be observed, as well, as if the added positive charges caused some

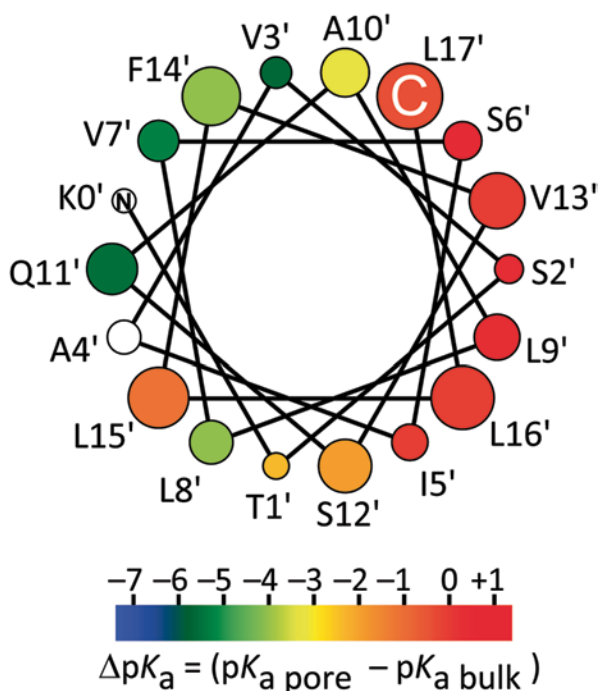


Fig. 8 ΔpK_a values mapped onto an ideal α -helical wheel representation of M2 of the AChR's δ subunit. The values corresponding to positions 2', 5', 6', 9', 13', 15', 16' and 17' were estimated using histidine substitutions; for all other positions (except for 0' and 4'), lysines were used. At positions 0' and 4', the presence or absence of basic side chains did not affect the single-channel conductance, and thus, their corresponding $pK_{a \text{ pore}}$ values could not be estimated (hence, the *white symbols*). The size of the symbols increases towards the extracellular end. Wild-type residues and the N and C termini are indicated. As judged from the deviations from bulk-water pK_a values, the data suggest that the (water-filled) lumen of the open-channel pore is to the right of the plot; importantly, this stripe of the α -helix is the same as that identified as lumen-facing on the basis of extent-of-block values (Fig. 5). The rather bulk-like pK_a value of a histidine at position 15' suggests the presence of an aqueous cavity in this region of the back of M2

inward rectification; three clear examples of this phenomenon are the lysine mutants at positions 9', 10' and 12' shown in Fig. 2b. Although we found that the magnitude of these shifts depends on the mutated position, we have not included the quantification of this variable in our analysis; thus far, we have only considered the extent to which the slope of the rectilinear portion of the i - V curves decreases upon protonation.

At some positions, neither the slope nor the displacement of the i - V curve along the voltage axis was affected upon the introduction of a basic residue (Fig. 5). This is the effect expected from positions in the protein that place the positively charged side chain either too far from the pore's lumen or in a microenvironment that shields the charge in such a way that the electrostatic effect is effectively screened (as would be the case for a highly hydrated region where water is less confined than in

Novel Chemical Tools to Study Ion Channel Biology

Ahern, C.; Pless, S. (Eds.)

2015, VIII, 154 p. 33 illus., 24 illus. in color., Hardcover

ISBN: 978-1-4939-2844-6